Interstellar Gas Flow Vector and Temperature Determination over 5 Years of IBEX Observations

Interstellar Gas Flow Vector and Temperature Determination over 5 Years of IBEX Observations

E. Möbius[1], M. Bzowski[2], S.A. Fuselier[3,4], D. Heirtzler[1], M. A. Kubiak[2], H. Kucharek[1], M.A. Lee[1], T. Leonard[1], D.J. McComas[3,4], N. Schwadron[1], J.M. Sokół[2], P. Wurz[5]

1   Space Science Center & Department of Physics, University of New Hampshire, Durham, NH 03824, USA
2   Space Research Centre, Polish Academy of Sciences, Warsaw, Poland
3   Southwest Research Institute, San Antonio, TX, USA
4   University of Texas, San Antonio, TX 78228, USA
5   Physikalisches Institut, Universität Bern, 3012 Bern, Switzerland

E-mail: Eberhard.moebius@unh.edu

Abstract. The Interstellar Boundary Explorer (IBEX) observes the interstellar neutral gas flow trajectories at their perihelion in Earth's orbit every year from December through early April, when the Earth's orbital motion is into the oncoming flow. These observations have defined a narrow region of possible, but very tightly coupled interstellar neutral flow parameters, with inflow speed, latitude, and temperature as well-defined functions of inflow longitude. The best-fit flow vector is different by $\approx 3°$ and lower by ≈ 3 km/s than obtained previously with Ulysses GAS, but the temperature is comparable. The possible coupled parameter space reaches to the previous flow vector, but only for a substantially higher temperature (by ≈ 2000 K). Along with recent pickup ion observations and including historical observations of the interstellar gas, these findings have led to a discussion, whether the interstellar gas flow into the solar system has been stable or variable over time. These intriguing possibilities call for more detailed analysis and a longer database. IBEX has accumulated observations over six interstellar flow seasons. We review key observations and refinements in the analysis, in particular, towards narrowing the uncertainties in the temperature determination. We also address ongoing attempts to optimize the flow vector determination through varying the IBEX spacecraft pointing and discuss related implications for the local interstellar cloud and its interaction with the heliosphere.

1. Introduction

The neutral gas component of the local interstellar cloud (LIC) that surrounds our solar system reaches the inner heliosphere as an interstellar neutral (ISN) wind due to the relative motion of the Sun and the interstellar material. On its way into the inner heliosphere the ISN wind composition and structure is altered on its passage through the heliospheric interface region, its flux is reduced by ionization losses, and its course is deflected by the Sun's gravitation and for H also by radiation pressure. This interaction of the surrounding interstellar medium with the heliosphere and its journey into the inner solar system has been described in numerous modeling studies, e.g. [1 – 5]. Among ISN constituents, He provides the most pristine sample of the surrounding LIC inside the heliosphere. Taking a sample of the LIC is important for a variety of reasons. In particular, the state of the LIC defines the boundary of

the heliosphere, it is the only accessible sample of cosmic bulk gaseous material other than from the solar system, and the Sun is currently located apparently at the edge of an interstellar cloud, with the prospect of exiting relatively soon on astronomical scales [6, 7] and a longer term history of dramatically changing interstellar conditions [8].

Local measurements of the ISN flow inside the heliosphere started with UV backscatter observations of H [9] and He [10], followed by pickup ion detection [11, 12], and finally neutral gas imaging of the flow itself [13, 14]. A concerted attempt to consolidate the measurements with these different optical and in-situ methods resulted in a set of consensus parameters for the LIC [15] and the realization that neutral gas imaging [16] should provide the most detailed and accurate information about the distribution function of the neutral gas in the LIC.

It came as a surprise that the first quantitative analysis of the ISN flow observations with the Interstellar Boundary Explorer (IBEX) [17, 18] appeared to suggest a different set of parameters, whose range included a different flow vector at its center with about the same temperature as found with Ulysses GAS [16] or at the edge of the range a similar flow vector, but with much higher temperature. Together with finding a larger interstellar magnetic field than before from the IBEX ENA observations [19], one potential consequence is the realization that the heliosphere likely has no fast bow shock [20]. The search for reconciliation of the different results, among others, has led to the proposal that the interstellar flow direction may have been changing over the course of the space age, supported by a compilation of 40 years of published interstellar flow direction results [21]. Stimulated by these intriguing possibilities, re-analysis efforts of the Ulysses GAS observations, including formerly unanalyzed data from the last fast latitude passage in 2007, are ongoing [22-24].

Recently, [25] have opposed the idea of a changing ISN flow by questioning the validity and interpretations of several of the results used in [21], albeit with several invalid arguments, which are addressed in [26]. In this paper, we will concentrate on the IBEX observations, firm up the temperature determination, and discuss the constraints that provide the IBEX flow vector values. The latter two have been called in question by [25] and yet are key to the IBEX analysis. We will also put the determination of the ISN flow vector into perspective with the interstellar magnetic field direction, derived among others from IBEX Ribbon observations [27-29]. Interstellar species, such as H and O, which are affected substantially by the heliospheric interface, should be deflected in a plane that is defined by the ISN inflow vector and the interstellar magnetic field direction [30-33]. The paper will close with a preview to IBEX observations with a modified spin axis orientation that should allow a more accurate determination of the ISN flow vector.

2. Instrumentation and Observations

IBEX was launched into a highly elliptical Earth orbit in October 2008 to observe energetic neutral atoms (ENAs) with minimum interference from the near Earth environment [34]. The satellite carries two single-pixel high-sensitivity ENA cameras, IBEX-Hi [35] and IBEX-Lo [36], whose fields-of-view (FoV) point perpendicular to the spin axis and whose combined energy range is $10 - 6000$ eV with overlap between 300 and 2000 eV.

IBEX-Lo has been optimized to observe interstellar H, He, and O flow distributions. Incoming neutral atoms pass a collimator, which determines the sensor FoV of 6.5° FWHM with regular resolution and 3.2° FWHM in high-resolution mode. The collimator and a set of repeller electrodes are biased to reject most of the ambient electrons and ions. After passing the collimator the neutral atoms are converted into negative ions on a highly polished conversion surface, which is covered with a vapor-deposited diamond-like carbon layer. The negative ions are then electrostatically collected into an electrostatic analyzer, where they are selected for energy, followed by post-acceleration in a potential of 16 kV (7 kV after summer 2012) and mass analysis in a triple-time-of-flight (TOF) section [36]. The triple TOF analysis also provides for superior rejection of noise and background contributions [37]. While H and O are detected and identified through the ready generation of converted H^- and O^- ions, noble gases, such as He and Ne, do not produce stable negative ions [38]. Therefore, these species are analyzed through negative ion sputter products of the carbon and an ever-present water layer,

which are produced with a combination of H^-, C^-, and O^- in characteristic proportions for each species and energy that was calibrated before flight. In particular, interstellar neutral (ISN) He produces a well characterized specific signature in IBEX-Lo [14, 18].

For each detected atom, energy step, TOF values, and a time tag with 4.2 ms resolution are registered in the form of individual events. The sensor also accumulates rates for each TOF and single detector. The events and rates are passed to a central electronics unit (CEU), which culls electron events due to their short TOF and accumulates histograms at 6° resolution in spin angle for atoms identified as H and O, separate for each of the 8 energy steps. Events with full information are buffered in the CEU and formatted into the telemetry. If the number of events exceeds the telemetry allocation, which occurs during the passage of the peak ISN flow, a sample of events is taken so that the full angle range is covered and preference is given to events with valid triple TOF detection over those with single TOF signals. Absolute rates for the angular distributions can be found through normalization to the H and O histograms [36].

Because IBEX-Lo provides energy bands with a resolution $\Delta E/E = 0.7$ and the energy information is almost completely lost for He in the sputter process, the detailed velocity distribution of the ISN flow is recovered from the observed angular distributions. IBEX is a roughly Sun-pointing, spinning satellite with the spin axis re-oriented towards the Sun after each 7–8 day orbit during the first three years and each half orbit arc of 4.6 days after raising the perigee into a lunar synchronous orbit in 2011 [39]. Complete full-sky ENA maps are obtained with a resolution comparable to the sensor FoV over a period of six months. As a consequence, IBEX samples the heliospheric and interstellar ENA distributions at 1 AU in a plane that is approximately perpendicular to the Earth-Sun line. This is equivalent to observing ENAs, which arrive from the heliospheric boundary or beyond, near the perihelia of their trajectories, regardless of their flow direction at infinity. This geometry allows significant simplification in the reconstruction of the flow distribution at infinity so that analytic approximations could be used in one of the analysis methods [40, 18]. However, the geometry also couples IBEX observables, and this coupling leads to a basic degeneracy in the observed parameters.

IBEX observes the ISN flow each year from late December through early April, when the Earth moves into the oncoming flow thus boosting the atom energy in the observer frame, with the passage of the He flow peak at ecliptic longitude $\lambda_{Peak} = 130.6 \pm 0.7°$ [18] around January 31. While the flow could, in principle, be also observed in the fall, when the Earth is overtaking the flow [41], the neutral atom energy in the spacecraft frame is too low, and no usable signal has been detected thus far.

3. Drivers for the Interstellar Flow Parameters

To understand the interstellar neutral gas flow vector and temperature results obtained by IBEX and their implications it needs to be reemphasized 1) which parameters are tightly coupled through the IBEX observables, 2) where the remaining degeneracy comes from, and 3) how it can be broken, although with an appreciably larger uncertainty. The end result of the coupling between the different LIC neutral gas parameters (flow longitude $\lambda_{ISM\infty}$, latitude $\beta_{ISM\infty}$, speed $V_{ISM\infty}$, and temperature $T_{ISM\infty}$) is a narrow "tube" of possible solutions in the 4-dimensional space of possible parameters. The three parameters ($V_{ISM\infty}$, $\beta_{ISM\infty}$, and $T_{ISM\infty}$) are related to $\lambda_{ISM\infty}$ (as independent variable) through a well-defined functional dependence, which because of its extension in $\lambda_{ISM\infty}$ constitutes a degeneracy due to the IBEX observation of the ISN flow over a limited portion of the Earth's orbit [17, 18, 20]. The "tube" of allowable values in velocity reaches to the velocity vector derived by [16] with Ulysses GAS, with a slightly differing combination in $\lambda_{ISM\infty}$, $\beta_{ISM\infty}$, and $V_{ISM\infty}$, but a noticeably different optimum $\lambda_{ISM\infty}$ and $V_{ISM\infty}$. As noted in the original papers, the IBEX vector could still be compatible with the Ulysses velocity within mutual uncertainties, but a substantially higher ($\approx 30\%$) ISN temperature is associated with the Ulysses velocity vector.

As discussed in [18] and [40], the determination of the ISN inflow vector is tied to the observation of the flux maximum (the ISN bulk flow vector at 1 AU) perpendicular to the Earth-Sun line with the Sun-pointing IBEX spacecraft (shown in Figure 1 for a sample ISN trajectory). Now $V_{ISM\infty}$ and $\lambda_{ISM\infty}$

are uniquely connected via the hyperbola equation for the true anomaly θ_∞ of the trajectory, which is related to bulk flow peak location λ_{Peak} at 1 AU and flow direction $\lambda_{ISM\infty}$ at infinity:

$$V_{ISM\infty} = \sqrt{\frac{GM_S}{r_E} \cdot \left(\frac{-1}{\cos(\theta_\infty)} - 1\right)} \quad \text{and} \quad \theta_\infty = \lambda_{ISM\infty} + 180^o - \lambda_{Peak} \tag{1}$$

The location of the flow maximum λ_{Peak} was determined independently with the same assumptions on ambient conditions [17, 18] to $\leq\pm0.7^o$, which constrains the functional relationship $V_{ISM\infty}(\lambda_{ISM\infty})$ in (1) to within $\leq\pm0.7^o$ in $\lambda_{ISM\infty}$ and $\leq\pm0.5$ km/s in $V_{ISM\infty}$. However, a large range of values along the function satisfies the observed ISN flow maximum at 1 AU equally well.

Simultaneously, functions for the ISN flow direction in latitude $\beta_{ISM\infty}(\lambda_{ISM\infty})$ and the temperature $T_{ISM\infty}(\lambda_{ISM\infty})$ can be obtained from the ISN flow peak location in latitude and its angular width. Because the statistical uncertainties of the peak location and angular width of the ISN flow are typically 2% and 1%, respectively, the combined uncertainties of the two relations are mostly controlled by the uncertainties in relation (1) and potential systematic effects, which we address for the derived temperature below. The observed angular distribution of the ISN flow constitutes a local Mach cone of width v_{Th}/V_{ISM_1AU}, with the bulk flow V_{ISM_1AU} and thermal speed v_{Th} at 1 AU, thus fixing the ratio $T_{ISM\infty}/V^2_{ISM\_1AU}$. In turn, $T_{ISM\infty}$ is tied to the adopted ISN speed $V_{ISM\infty}$ and thus to $\lambda_{ISM\infty}$.

As shown in Figure 1, the flow latitude Ψ_{Peak} at 1 AU in the rest frame is connected to the ISN flow latitude $\beta_{ISM\infty}$ at infinity through the true anomaly of the bulk flow as

$$\tan(\psi_{Peak}) = \frac{\tan(\beta_{ISM\infty})}{|\sin(\theta_\infty)|} = \frac{\tan(\beta_{ISM\infty})}{|\sin(\lambda_{ISM\infty} + 180^o - \lambda_{Peak})|} \tag{2}$$

and thus again to the ISN inflow longitude $\lambda_{ISM\infty}$. These relations constitute a degeneracy in the determination of $V_{ISM\infty}$, $\beta_{ISM\infty}$, and $T_{ISM\infty}$ as a function of $\lambda_{ISM\infty}$. However, relation (2) also provides the means to break the degeneracy with IBEX observations. When latitude distributions are combined for different longitude λ_{Obs} positions with IBEX as observer, then, λ_{Obs} replaces λ_{Peak} in Equation (2). With λ_{Obs} now as a variable, the resulting relation $\Psi_{Peak}(\lambda_{Obs})$ depends solely on $\lambda_{ISM\infty}$. The comparison of ISN flow distributions observed over entire observation seasons with the predicted relation (2) as a function of $\lambda_{ISM\infty}$ and respective χ^2-minimization in [18] resulted in the reported optimum inflow longitude $\lambda_{ISM\infty} = 79^o +3.0^o(-3.5^o)$. Independently, [17] obtained a similar result through numerical modeling. The uncertainties in $\lambda_{ISM\infty}$ are the basis for the bounding values of the resulting parameter range from the IBEX observations used in [20].

To illustrate the basis for the inflow direction in the IBEX analysis, the right panel in Figure 1 shows the peak location of simulated ISN flow distributions in latitude Ψ_{Peak} for the usable observation
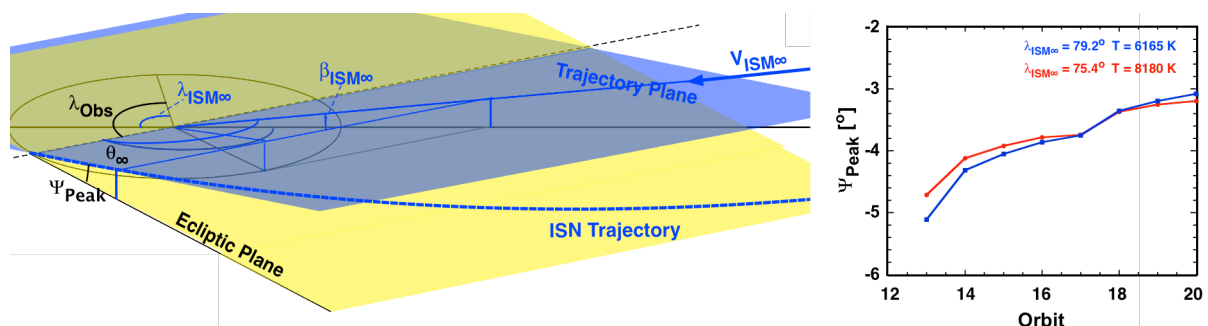

Fig. 1: ISN flow trajectory in its orbit plane (blue), which intersects the ecliptic plane (yellow) along the observer-Sun line and is inclined by the angle Ψ_{Peak} of the observed flow peak (shown in the inertial frame). The ISN flow vector at infinity $V_{ISM\infty}$ is inclined by the inflow latitude $\beta_{ISM\infty}$. The local peak flow angle Ψ_{Peak} varies with the true anomaly θ_∞ of the trajectory and thus with observer location λ_{Obs} and inflow longitude at infinity $\lambda_{ISM\infty}$. The right panel shows the simulated variation $\Psi_{Peak}(\lambda_{Obs})$ as averages over the 2009 IBEX orbits for $\lambda_{ISM\infty} = 75.4^o$ and 79.2^o.

periods during the 2009 ISN season orbits. Shown are the results for two ISN flow parameters sets on the center line of the parameter tube as defined in equations (1) and (2), using the flow longitude $\lambda_{ISM\infty}$ of [16] (red) and that of [17, 18] (blue). The visible difference between the two curves with different $\lambda_{ISM\infty}$ along the IBEX tube is a steeper variation of Ψ_{Peak} as a function of orbit (longitude) towards earlier orbits, for the $\lambda_{ISM\infty}$ value stated in [17, 18] over that in [16]. The optimization used in [18] is solely sensitive to the shape of the curves in Figure 1. The shape of these curves also dominates the χ^2-minimization for simulated flow distributions in [17], but this method is also sensitive to the overall shape of the observed angular distributions.

4. Temperature Determination

The temperature required by the IBEX relations for the velocity vector of [16] is much higher than reported there. The authors of [19] argue that the width of the angular distribution, which now solely influences the derived temperature, could be brought into agreement with the Ulysses temperature value by assuming unknown instrumental effects in IBEX. We have determined $T_{ISM\infty}$ from the width of the latitude distribution in the analytic method [18]. The value obtained through χ^2-minimization by [17] is also dominated by the latitudinal variation of the fluxes. The left two panels of Figure 2 show angular distributions in latitude for the two peak orbits in 2009 and 2010 that have been mainly used to determine the He temperature in [18]. We show 2048-spin accumulations here for two time periods that are selected for almost identical ecliptic longitude close to the ISN flow maximum, as constrained by the ISN good times according to [18] for these orbits (Table 1 in [18]). Identical longitude is very important for comparable widths as can be seen in the right panel, which shows the width obtained from every second 512-spin period during ISN good times of orbit 64. The width decreases by $\approx 0.7°$ over the course of 7 days or 7° in longitude. Given this variation, the angular widths obtained in 2009 and 2010 are in remarkable agreement. To match the ISN flow maximum longitude (130.6±0.7°) in the temperature determination, [18] combined these orbits with the previous ones. The data used in Figure 2 are made available as 512-spin (≈ 2 hour) time periods for the ISN flow good times, as in Table 1 of [18], under IBEX Data Release 6 (http://ibex.swri.edu/researchers/publicdata.shtml#dr6). The angular distributions are provided in 6° resolution, with both the sum of direct and histogram events listed for full correction of the telemetry limitations, similar to Data Release 3 with longer time intervals.

As discussed in [18] the peak height and thus the width of these distributions as shown in Figure 2 could be affected by particle rate dependent suppression of the data flow of individual events through the CEU. In such a case, the peak of an angular distribution would be reduced the most, thus increasing the apparent width of the original angular distribution. To account for such potential, at the time
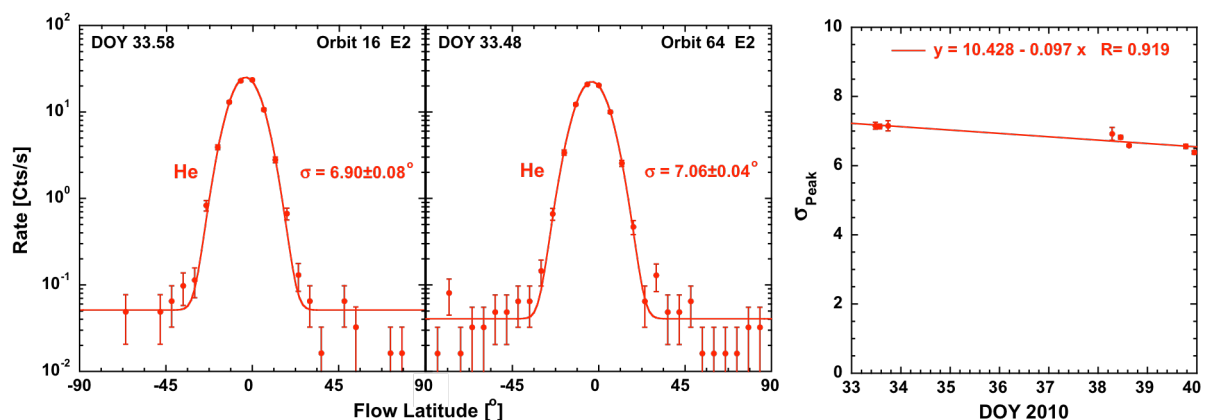

Fig. 2: Left: Latitude distributions for two 2048-spin periods in orbits 16 and 64 from ISN flow good times [18] that are only 0.3° in ecliptic longitude apart (orbit 64 is 0.3 days earlier or 0.3° closer to 0°) with Gaussian fit and statistical error bars. Right: Derived width after subtracting the collimator function as a function of time over orbit 64 taken over every second 512-spin period during the ISN flow good times. The angular width decreases as a function of time and thus ecliptic longitude.

unknown, effects [18] estimated an upper limit in terms of a maximum CEU event processing time $\tau \leq$ 5 ms. They modeled the processing analytically similar to a dead time and compared observations of the ISN flow at IBEX-Lo energy steps 2 and 4, the latter with a rate lower by a factor of 5 and thus much reduced interface traffic. In [19] the authors claim that an instrumental dead time $\tau \approx 7$ ms would allow reconciliation of the angular distributions observed with Ulysses and IBEX, although [18] indicated that $\tau \leq 5$ ms is an upper limit and [20] reported that the effect on the width and thus the temperature was much smaller based on follow-up testing and simulation, as discussed in more detail below.

The telemetry limitation for high-flux neutral atom sources, such as the ISN flow and the Earth's magnetosphere, was anticipated in the IBEX mission planning, and therefore H and O energy-angle histograms with 6° resolution are accumulated onboard IBEX to normalize the reported event rates. Because the width of the IBEX-Lo FoV is already 6.5° FWHM and to eliminate any potentially unanticipated effects on the data flow by the limited telemetry at angular resolution <6°, [17] and [18] restricted the angular resolution to 6°, thus using the histograms (accumulated in the CEU) for full correction of any telemetry limitations and their effects.

In addition, the hardware interface between IBEX-Lo and the CEU has a known transfer time of 1.354 ms for each event, which increases for the first 1° of each 6° bin to 2.188 ms because IBEX-Lo housekeeping and rates are also transmitted. Both transmission times are much shorter than the previously estimated maximum processing time. The response of the interface to a large variety of event rate combinations was verified with a hardware simulator and computed in Monte Carlo simulations. We found that the majority of the events transmitted by the interface (typically 300–400 s^{-1}) originate from an unanticipated substantial electron flux through the sensor mentioned by [18]. These electron events, along with other events that fall outside the TOF criteria for either H or the combination of C and O, are all fed into the CEU for selection. While electrons are readily identified based on their short or missing TOF signals and completely eliminated from ENAs, they still load the interface with a base traffic. However, because the ISN flow distributions contribute only a small fraction ($\leq 20\%$) to the total interface traffic, the effect on the shape of these distributions is very small. A change of the sensor mode in mid 2012 excludes the majority of these events that do not have any valid TOF signal by explicitly requiring the presence of at least the TOF between the two carbon foils. After that mode change the interface load has no noticeable effects on the data flow anymore

Figure 3, which shows two consecutive angular distributions of the ISN flow taken early February 2013 in the new IBEX-Lo mode (TOF2 required, left panel) and in the original normal mode (no TOF required, right panel), demonstrates the overall data flow reduction of the peak rate that is $\approx 20\%$ reduced in the old mode, but no noticeable broadening of this distribution in comparison with the other distribution. Contrary to expectation, the width in the old mode, (σ after subtraction of the collimator function) appears even slightly smaller (by 0.32°), 0.13° of which may be attributed to the fact that this angular distribution is taken ≈ 1.3 days later when the ISN flow distribution is already slightly narrower (c.f. Figure 2). Also, simulations have demonstrated that in the old mode the potential increase in width of the observed angular distributions is limited to at most 1%, or to an apparent increase in the
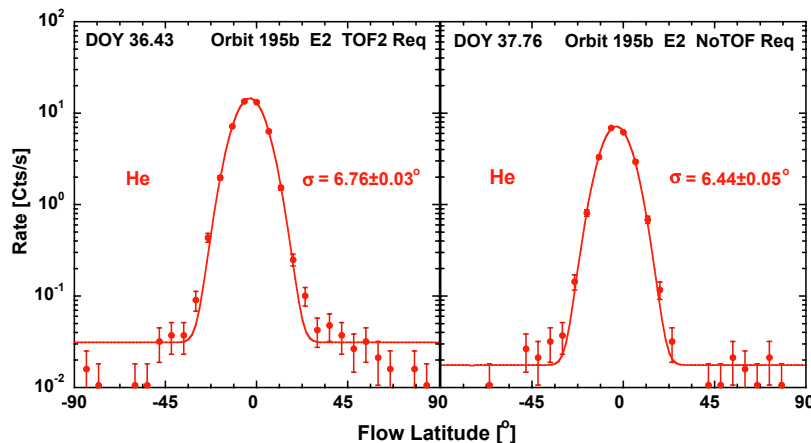

Fig. 3: Latitudinal distribution for the entire time period when IBEX-Lo was returned to the mode used 2009 to mid 2012 (right) together with an equally long time period in the new mode that removes all events with no valid TOF signal from the traffic into the CEU (left). Although added traffic tends to reduce the event rate (by $\approx 20\%$) the angular width is slightly smaller, 0.13° of which may be attributed to the 1.3 days later time.

deduced temperature of <2%, as fully supported by the comparison in Figure 3. Therefore, any systematic instrumental effects on the temperature determination from IBEX observations larger than 2% can be excluded for the observations analyzed thus far.

In addition, we have tested whether broad non-uniform background, for example, from a secondary neutral helium component underneath the ISN flow distribution could lead to a broader combined distribution. The higher temperature observed by IBEX would require the addition of a component with at least 15% of the ISN flow peak height, which would be visible in large non-thermal wings that are not observed. Therefore, such an effect is also excluded.

Figure 4 shows the inflow speed and temperatures of He and the O and Ne combination obtained with IBEX [17, 18, 20] as a function of $\lambda_{ISM\infty}$ along the resulting narrow tube in LIC parameter space. T_{He} is now shown with only a 2% reduction over the width of the measured distribution, reflecting the maximum effect on the data flow, i.e. much less than the combined error bar. The lower reduction reflects the current understanding of the effect of the electron TOF events on the overall ISN signal. The temperatures of the different LIC species are in agreement within their respective error bars. This agreement provides another argument against substantial instrumental effects in the temperature because these would not likely lead to the observed isothermal result. The 1-σ range in $\lambda_{ISM\infty}$ as obtained in [18] and [17] along the parameter tube is indicated by open triangles, and the center value is indicated by the open squares. For comparison, the LIC parameters in [16] are also shown with their error bars. While the $V_{ISM\infty}(\lambda_{ISM\infty})$ combination falls at the edge of the IBEX range as reported before, the Ulysses temperature is substantially lower.
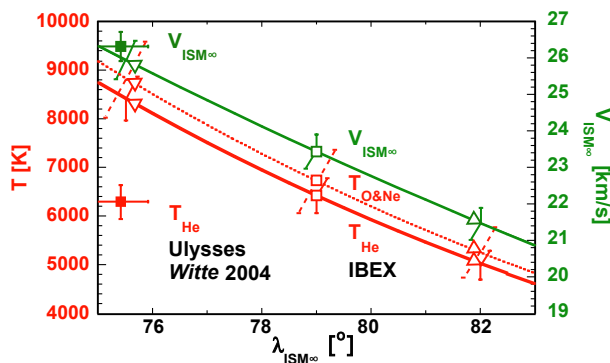

Fig. 4: ISN inflow speed $V_{ISM\infty}$ and temperatures T_{He} and $T_{O\&Ne}$ as a function of flow longitude $\lambda_{ISM\infty}$ obtained with IBEX [17, 18, 20] with error bars perpendicular to the parameter tube. The ranges along the tube are indicated by open triangles and the center value by open squares. Ulysses GAS values (solid squares) from [16] are shown in J2000 coordinates with the respective error bars.

5. Other Consequences and Future Perspectives

As has been demonstrated in the previous sections and in accordance with earlier results in [17, 18, 20], the IBEX ISN observations lead to a narrow tube of parameters for the LIC velocity vector and temperature, for which $V_{ISM\infty}$, $\beta_{ISM\infty}$, and T_{ISM} can be expressed as unique functions of $\lambda_{ISM\infty}$. Driven mostly by the observed variation of the flow peak in latitude as a function of observer longitude, a best fitting ISN flow longitude $\lambda_{ISM\infty} = 79°$ is found [20], although the range in longitude along the tube reaches all the way to the previously favored value $\lambda_{ISM\infty} = 75.4°$ (in J2000 coordinates [15, 16]). Interestingly, the flow longitude favored by the IBEX observations results in a LIC temperature $T_{ISM} = 6300\pm360$ K as also reported in [15, 16], while lower longitudes are tied to increasing temperatures, with $T_{ISM} = 8300\pm450$ K for $\lambda_{ISM\infty} = 75.4°$ as a consequence of the local Mach cone measurement. We have excluded instrumental effects and the influence of non-uniform backgrounds as potential reasons for observing substantially higher temperatures with IBEX than with Ulysses GAS. In addition, the IBEX angular distributions that are used to determine the temperature from their width are obtained with much superior counting statistics, and the ISN O+Ne temperature is the same within mutual error bars. Therefore, the relation found for the LIC temperature with IBEX appears very solid.

When putting these results into context, several intriguing possibilities arise. Firstly, the vector favored by the IBEX results appears to agree better with the LIC velocity vector in [42], who argued based on the local ISN velocity from [15, 16] and their cloud velocities that the heliosphere might be

in a transition region between the LIC and the G-cloud. Secondly, together with a trend found over the entire space age, the possibility of a change in the interstellar flow vector over time, as proposed by [21] cannot be simply dismissed, as suggested in [25]. In such a scenario, the Ulysses GAS results by [16] and the IBEX observations would be consistent with sampling the same LIC temperature, but different velocity vectors, or encountering different portions of turbulent eddies at the edge of the LIC, where astronomical studies place the solar system [6, 7]. Alternatively, and this may be born out in more recent analyses of GAS observations [23, 24] and more extended IBEX observations, the local LIC flow vector could consolidate to values that are in agreement, but with higher LIC temperatures than previously found with GAS. LIC temperatures determined by absorption line measurements show values between ≈5800 and ≈10,000 K [26]. Because these represent a variety of line-of-sight averages, the local observation in the heliosphere could point to a locally higher temperature, perhaps, at the edge of the LIC.

An accurate determination of the pristine LIC flow vector is important also for another reason. Already [17] pointed out that a relatively subtle change in inflow longitude by ≈3° over the previous value has drastic consequences when taken in context with the inflow direction of ISN H as reported by [30, 43], which is deflected from the pristine flow direction due to the draping of the interstellar magnetic field B_{ISM} over the heliosphere [31-33]. According to global heliospheric modeling [32], the direction in the sky, into which the H flow is deflected, is determined by the orientation of the B_{ISM}-$V_{ISM\infty}$ plane. The relatively substantial change of the B_{ISM}-$V_{ISM\infty}$ plane orientation in the sky caused by a 3° change in $\lambda_{ISM\infty}$ is illustrated in the left panel of Figure 5. The most accurate determination of the B_{ISM} direction can be expected from the location of the IBEX ribbon, which has been interpreted within most models [27, 28, 44] as showing the locus in the sky where $\vec{B}_{ISM} \cdot \vec{r} = 0$ holds, preferably with solar wind involvement [45-47]. The most accurate determination of the ribbon center, which according to these models represents the up- or down-field direction in the sky, is from [29]. As discussed by [48] in terms of a secondary ENA model [45, 47], higher energy ribbon ENAs would probe larger distances from the Sun and thus should represent progressively more pristine interstellar conditions. The ribbon center as the B_{ISM} direction has been validated recently based on the streaming direction inferred from TeV cosmic ray anisotropies [49]. Shown in the right panel of Figure 5 are the ribbon centers for different ENA energies, along with the nose direction and the orientation of the B_{ISM}-$V_{ISM\infty}$ plane for the LIC velocity vectors from Ulysses GAS and IBEX. The Ulysses GAS result is more closely aligned with the expected B_{ISM} direction at the lower ENA energies, while the IBEX result agrees better with the direction from higher energies. Therefore, an accurate determination of the LIC inflow vector will be of utmost importance for probing the outer heliosheath where B_{ISM} controls the flow pattern around the heliosphere.
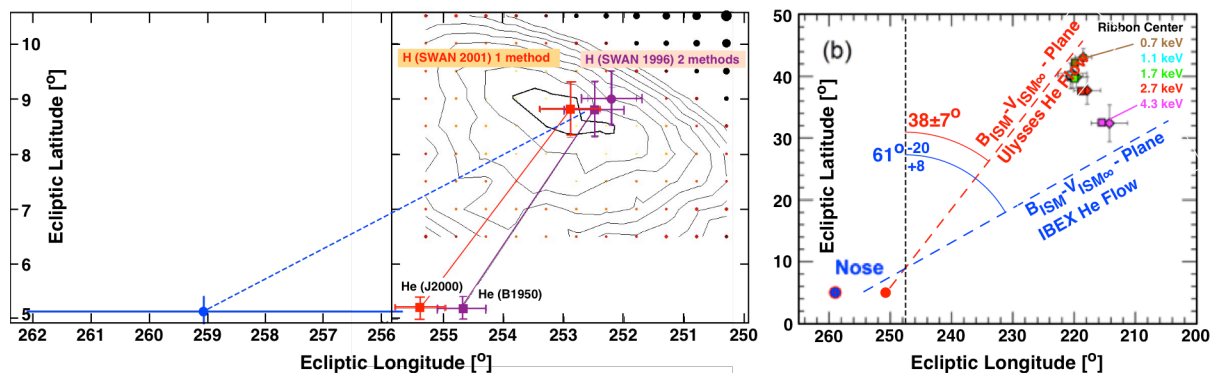

Fig. 5: Left Panel: Flow direction of ISN H from SOHO SWAN [43] and of He from Ulysses GAS (red [16]) and IBEX (blue [17, 18] along with projected B_{ISM}-$V_{ISM\infty}$ - planes (adapted from [43]). Right Panel: IBEX ribbon center locations in the sky for different ENA energies [29] along with the heliospheric nose and projected B_{ISM}-$V_{ISM\infty}$ - planes based on Ulysses and IBEX observations.

To provide improved leverage to IBEX observations in breaking the inherent degeneracy along the narrow LIC parameter tube, the IBEX team has started with a variation in the pointing of the IBEX spin axis to substantial negative latitudes, as a means to uniquely identify where in the four-dimensional parameter space tube the ISN flow actually lies. Figure 6 shows how the observed ISN flow peak in latitude at a given observer longitude varies as a function of inflow longitude for different IBEX spin axis orientations. Generally, a spin axis pointing below the ecliptic (more negative values in e_z) results in a steeper functional behavior and thus provides stronger leverage on the determination of the ISN inflow longitude. In 2014, the observations were made with a spin axis orientation of $\approx$-5°, interspersed with an axis orientation of $\approx$0°. The new observations are currently under evaluation.
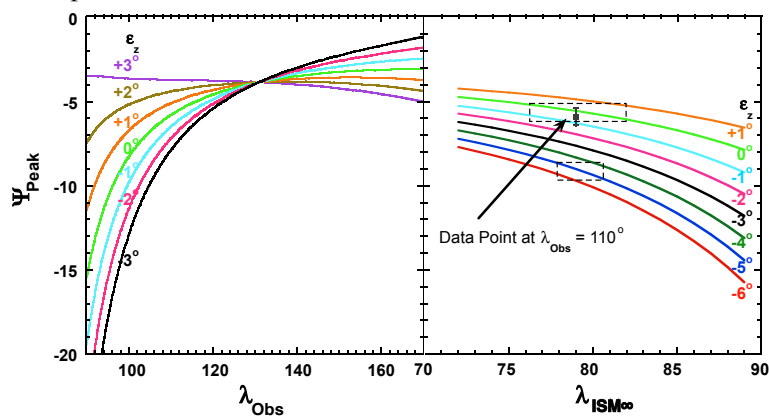

Fig. 6: ISN Flow peak location in latitude Ψ_{Peak} as a function of observer longitude λ_{Obs} (left) and as a function of $\lambda_{\text{ISM}\infty}$ for $\lambda_{\text{Obs}} = 110^{o}$ (right) with different spin axis orientations ε_z. The ability to discern $\lambda_{\text{ISM}\infty}$ by exploiting the variation of Ψ_{Peak} with λ_{Obs} is improved with progressively steeper functional dependence for more negative spin axis pointing. Included in the right panel are a typical data point with error bar and resulting error boxes in $\lambda_{\text{ISM}\infty}$ for $\varepsilon_z = 0^{o}$ (2012&13) and -5° (2014).

6. Conclusions

IBEX observations of the ISN He flow during early winter each year provide a versatile tool to determine the physical parameters of the LIC, with the potential for continuing improvement with multiple data sets and varying observation strategies. Multiple year observations have confirmed the narrow tube of LIC parameters $V_{\text{ISM}\infty}$, $\beta_{\text{ISM}\infty}$, and $T_{\text{ISM}}(\lambda_{\text{ISM}\infty})$ with small error bars perpendicular to these functional dependencies and a larger uncertainty around the center value of $\lambda_{\text{ISM}\infty} = 79^{+3}_{-3.5}{}^{o}$ (c.f. Fig. 4). In particular, the T_{ISM} values have been solidified in a detailed analysis of the IBEX data path, which has shown that the observed angular distributions may only be widened by $\leq$1% (or T_{He} by $\leq$2%) in the worst-case scenario. Therefore, the He temperature found from IBEX observations is $\approx$30% higher than that reported in [16] when adopting the same ISN flow vector. Recent re-analyses of the Ulysses GAS observations point to an underestimate of the temperature in the earlier analysis [23, 24].

We have combined the Ulysses GAS and the IBEX ISN flow vectors with the determination of the H ISN flow from SOHO SWAN observations as shown in [43] and compared the resulting B_{ISM}-$V_{\text{ISM}\infty}$ planes with the B_{ISM} direction as derived from the IBEX ribbon center, following models that connect the ribbon location to the locus where $\vec{B}_{\text{ISM}} \cdot \vec{r} = 0$ is satisfied. Then the plane derived with the Ulysses direction is nearly in line with the ribbon center at 0.7 keV, while the IBEX direction agrees better with the ribbon center at the highest energy 4.2 keV, as derived in [29]. In terms of a secondary ENA model for the ribbon, the center at higher energies would come closer to a B_{ISM} direction at larger distances [48], i.e. supposedly under more pristine (undraped) conditions. This presents one more reason to derive the ISN flow vector with higher precision. To achieve this goal, the IBEX spin axis orientation has been turned to larger negative latitude, which promises a better sensitivity of the observations to the inflow longitude, which is still most uncertain in the IBEX analysis.

References

[1]   Fahr, H., Kausch, T. & Scherer, H. 2000, *A&A* **357**, 268.

[2]   Zank, G.P., & Müller, H.R., 2003, *JGR* **108**, 1240.

[3]   Alexashov, D. & Izmodenov, V. 2005, *A&A* **439**, 1171.

[4]   Müller, H., Florinski, V., Heerikhuisen, J., et al. 2008, *A&A* **491**, 43.

[5]   Zank, G., Pogorelov N., Heerikhuisen J., et al. 2009, *Space Sci. Rev.* **146**, 295.

[6]   Cheng, K, & Bruhweiler, F., 1990, *ApJ* **364**, 573.

[7]   Slavin, J., & Frisch, P., 2002, *ApJ* **565**, 364.

[8]   Frisch, P. C., 2006, *Solar Journey*, vol. 338, Dordrecht: Springer.

[9]   Bertaux, J., & Blamont, J., 1971, *A&A* **11**, 200.

[10]   Weller, C., & Meier, R., 1974, *ApJ* **193**, 471.

[11]   Möbius, E., Hovestadt, D., & Klecker, B., 1985, *Nature* **318**, 426.

[12]   Gloeckler, G., Geiss, J., Balsiger, H., et al., 1992, *A&A* **92**, 267.

[13]   Witte, M., Banaszkiewicz, M., & Rosenbauer, M., 1996, *Space Sci. Rev.* **78**, 289.

[14]   Möbius, E., Bochsler, P., Bzowski, M., et al. 2009a, *Science* **326**, 969.

[15]   Möbius, E., Bzowski, M., Chalov, S., et al. 2004, *A&A* **426**, 897.

[16]   Witte, M., 2004, *A&A* **426**, 835.

[17]   Bzowski, M., Kubiak, M., Möbius, E., & et al., 2012, *ApJS* **198**, art ID 12.

[18]   Möbius, E., P. Bochsler, M. Bzowski, et al., 2012, *ApJS* **198**, art ID 11.

[19]   Schwadron, N. A., Allegrini, F., Bzowski, M., et al. 2011, *ApJ* **731**, 56.

[20]   McComas, D.J., Alexashov, D., Bzowski, M., et al., 2012, *Science* **336**, 1291.

[21]   Frisch, P. C., Bzowski, M., Livadiotis, G., et al., 2013, *Science* **341**, 1080.

[22]   Katushkina, O., A., Izmodenov, V.V., Wood, B.E., McMullin, D.R., *ApJ*, in press, 2014.

[23]   Bzowski, M., et al., 2014, *ApJ*, subm..

[24]   Wood, B., Mueller, H.-R., & Witte, M., 2014, *ApJ*, subm.

[25]   Lallement, R., & Bertaux, J.L., 2014, *A&A* **565**, id.A41..

[26]   Frisch, P.C., Bzowski, M., Drews, C., et al., 2014, *ApJ*, subm..

[27]   McComas, D. J., Allegrini, F., Bochsler, P., et al. 2009a, *Science* **326**, 959.

[28]   Schwadron N A, Bzowski M, Crew G B, et al., 2009, *Science* **326,** 966.

[29]   Funsten, H., R. DeMajistre, P. C. Frisch, et al., *ApJ* **776**, Art ID 30, 2013.

[30]   Lallement, R., Quemerais, E., Bertaux, J. L., et al., 2005, *Science* **307**, 1447.

[31]   Izmodenov V.V., Alexashov D.B., Myasnikov A.V., 2005, *A&A* **437**, L35.

[32]   Pogorelov, N. V., Heerikhuisen, J., Mitchell, J. J., et al., 2009, *ApJ. Lett.* **695**, 31.

[33]   Opher, M., Stone, E. C. , Gombosi, T., 2007, *Science* **316**, 875.

[34]   McComas, D. J., Allegrini, F., Bochsler, P., et al. 2009b, *Space Sci. Rev.* **146**, 11.

[35]   Funsten, H. O., Allegrini, F., Bochsler, P., et al. 2009, *Space Sci. Rev.* **146**, 75.

[36]   Fuselier, S., Bochsler, P., Chornay, D., et al., 2009, *Space Sci. Rev.* **146**, 117.

[37]   Wurz, P. S.A. Fuselier, E. Möbius, et al., 2009, *Space Sci. Rev.* **146**, 173.

[38]   Hotop, H., & Lineberger, W.C., 1984, *J. Phys. Chem. Ref. Data* **14**, 731.

[39]   McComas, D.J., Carrico, J.P., Hautamaki, B., et al., 2011, *Space Weather* **9**, CiteID S11002.

[40]   Lee, M., Kucharek, H., Möbius, E., et al., 2012, *ApJS* **198**, art ID 10.

[41]   Möbius, E., Kucharek, H., Clark, G., et al. 2009b, *Space Sci. Rev.* **146**, 149.

[42]   Redfield, S., & Linsky, J., 2008, *ApJ* **673**, 283.

[43]   Lallement, R., Quemerais, E., Koutroumpa, D., et al., 2010, *AIP Conf. Proc.* **1216**, 555.

[44]   McComas, D.J., Lewis, W.S., & Schwadron, N.S., 2014, *Rev. Geophys.* **52**, doi:10.1002/2013RG000438.

[45]   Heerikhuisen, J., Pogorelov, N. V., Zank, G. P., et al., 2010, *ApJ Lett.* **708**, L126.

[46]   Kucharek, H., Fuselier, S.A., Wurz, P., et al., 2013, *ApJ* **776**, art ID 109..

[47]   Schwadron, N. A. & McComas, D. J., 2013, *ApJ* **764,** 92.

[48]   Möbius, E., K. Liu, H. Funsten, S. P. Gary, D. Winske, 2013, *ApJ* **766**, art ID 129.

[49]   Schwadron, N. A., Adams, F. C., Christian, E. R., et al., 2014, *Science* **343,** 988.